Unexpected symmetry and AA stacking of bilayer silicene on Ag(111)

Paul Pflugradt,* Lars Matthes, and Friedhelm Bechstedt

Institut für Festkörpertheorie und -optik, Friedrich-Schiller-Universität and European Theoretical Spectroscopy Facility (ETSF), Max-Wien-Platz 1, 07743 Jena, Germany

(Received 3 February 2014; revised manuscript received 10 April 2014; published 22 May 2014)

We report results of *ab initio* density functional theory including van der Waals interaction for the formation of a silicene bilayer on top of the Ag(111) surface with significant differences to the monolayer case. We find $(2\sqrt{3} \times 2\sqrt{3})R30^\circ$ bilayer silicene on $(\sqrt{19} \times \sqrt{19})R23.4^\circ$ silver substrate to be the most stable. The calculated STM images, however, exhibit a $(\sqrt{3} \times \sqrt{3})R30^\circ$ symmetry. This translational symmetry, the resulting lattice spacing, and the height of the topmost monolayer agree with recent experimental findings. The band structure of the complete adsorbate system shows conical linear bands near the Fermi level due to the hybridization of adsorbate and substrate states.

DOI: 10.1103/PhysRevB.89.205428 PACS number(s): 73.20.Hb, 68.43.Bc, 73.22.Pr, 81.05.Zx

I. INTRODUCTION

The honeycomb symmetry of a two-dimensional (2D) layer of group-IV atoms exhibits peculiar electronic properties with conical linear bands and, hence, the appearance of massless Dirac fermions near the Fermi energy [1]. One consequence is the constant infrared absorbance ruled by the Sommerfeld fine-structure constant [2]. A possible realization of such a 2D system is the graphenelike allotrope of silicon, silicene, which however is buckled and partly sp^3 bonded, in contrast to graphene. However, no Si-based layered crystal similar to graphite exists in nature. Therefore, substrates are indispensable for growing or depositing silicene sheets.

Recently several experimental groups reported the epitaxial growth of silicene on Ag(111) surfaces [3–10]. In angle-resolved photoemission spectroscopy (ARPES) measurements [3,9,10], but also by mapping of differential conductance [5], the existence of Dirac cones of massless fermions has been claimed. This fact is, however, controversially discussed [11–17]. Very recently, in multilayer silicene seemingly with a $(\sqrt{3} \times \sqrt{3})R30^\circ$ translational symmetry, massless Dirac-Weyl fermions in Si-derived systems were measured by means of ARPES near the Γ point. Linear bands were found and interpreted as experimental proof of massless fermions [10]. It is suggested that the corresponding bilayer system is grown by adding another $\sqrt{3} \times \sqrt{3}$ reconstructed layer on top of the 3×3 silicene monolayer on a Ag(111)4×4 substrate. However, the atomic geometry of the silicene bilayer as well as its interaction with the substrate are completely unknown. This fact also holds for their relationship to the electronic structure such as scanning tunneling microscopy (STM) images, local density of states, and band structures. Corresponding studies of bilayer and multilayer silicene are completely missing.

In this paper we focus on bilayer silicene on an Ag(111) substrate, by means of extensive density functional theory (DFT) calculations including van der Waals (vdW) interaction. We investigate the stability of bilayer silicene dependent on stoichiometry, reconstruction, and symmetry. We predict a $(2\sqrt{3} \times 2\sqrt{3})R30^\circ$ adsorbate on a $(\sqrt{19} \times \sqrt{19})R23.4^\circ$ substrate, i.e., translational symmetries which are not observed in the monolayer case. The driving forces are discussed in detail. The seemingly $(\sqrt{3} \times \sqrt{3})R30^\circ$ translational symmetry observed by STM and low-energy electron diffraction (LEED) experiments [18,19] are explained as well as the resulting STM images and bands near the Fermi energy.

II. METHODOLOGY

The structural optimization and total-energy calculations are performed within the DFT as implemented in the Vienna *ab initio* simulation package (VASP) [20]. The vdW interaction is included according to Dion *et al.* [21]. The details of the implementation of the vdW functional including the local-density treatment of correlation and the exchange description within generalized-gradient approximation are described by Klimeš *et al.* [22]. Despite the underestimation of the Fermi velocity of freestanding silicene [23], the resulting electronic structure is sufficient to demonstrate the appearance of characteristic electronic features like Dirac cones. The pseudopotentials are generated using the projector-augmented wave (PAW) method [24]. The Kohn-Sham eigenvalues and eigenfunctions are applied to compute STM images and electronic band structures.

The Ag(111) substrate is simulated by periodic arrangements of symmetric slabs which are separated by a vacuum region of 15 Å. The slabs consist of nine substrate layers with a lateral (surface) lattice constant of $a = 3.86$ Å. The initial atomic configurations are constructed by adding silicene layers symmetrically on both slab sides. For proper translational symmetries of the silver surface and the silicene layers, coincidence lattices [25] are constructed. All Si atoms and one Ag layer on both sides of a slab are allowed to relax until the Hellmann-Feynman forces are below 1 meV/Å. The Brillouin zone (BZ) of the repeated slab system is sampled by a $6 \times 6 \times 1$ **k**-point mesh. STM images are computed within the constant-current mode using the Tersoff-Hamann approach [26].

III. RESULTS AND DISCUSSION

A. Atomic geometries

The construction of reasonable starting geometries for the total-energy optimization of bilayer systems is difficult,

*paul.pflugradt@uni-jena.de

since the available experimental data mainly give information about the topmost silicene layer. The $\sqrt{3} \times \sqrt{3}$ honeycomb symmetry of the topmost silicene layer on Ag(111) was observed in several STM, ARPES, and LEED experiments [5,9,10,18,19]. The most recent STM studies [10] clearly display the coexistence of 3×3 monolayers (MLs) with bilayer (BL) islands (and thicker ones) with $\sqrt{3} \times \sqrt{3}$ symmetry. A few experiments suggest the growth of $(\sqrt{3} \times \sqrt{3})R30^\circ$ reconstructed layers on top of the first 3×3 reconstructed silicene wetting layer on Ag(111)4×4 substrates [9,10]. However, this suggestion is based on the interpretation of STM images and static diffraction spots in LEED. The atomic structure of the silicene bilayer, in particular the second layer, remains unknown from these experiments.

We have performed an extensive search for stable geometries of bilayer silicene on Ag(111) with various translational symmetries. As a clear result, the deposition of an additional $\sqrt{3} \times \sqrt{3}$ ML on a 3×3 silicene/4×4 Ag(111) system does not lead to a BL structure with $\sqrt{3} \times \sqrt{3}$ translational symmetry. In fact, all four stable monolayer translational symmetries $(\sqrt{7} \times \sqrt{7})R19.1^\circ$ on $(\sqrt{13} \times \sqrt{13})R13.9^\circ$, 3×3 on 4×4, 2×2 on $(\sqrt{7} \times \sqrt{7})R19.1^\circ$, and $(\sqrt{7} \times \sqrt{7})R19.1^\circ$ silicene on $(2\sqrt{3} \times 2\sqrt{3})R30^\circ$ silver(111) (see Ref. [27]) do not form a top layer with $\sqrt{3} \times \sqrt{3}$ symmetry if a second silicene layer is added. Merely in the 3×3 on 4×4 case, the 3×3 unit cell can decay directly in four $\sqrt{3} \times \sqrt{3}$ cells. Therefore, all other structures were tested with nonstoichiometric bilayer silicene. In all calculations we observed significant atomic rearrangements of the underlying atomic layers during the relaxation. The geometry of the wetting-layer silicene is destroyed by a substantial Si-Si interaction; Si atoms even leave the previously preferred high-symmetry positions of the underlying silver. Starting from known monolayer geometries, no $\sqrt{3} \times \sqrt{3}$ translational symmetry of the BL system is found.

We observed a pronounced tendency toward the rearrangement of the Si atoms in the upper silicene on top of occupied sites in the lower silicene monolayer. In other words, an AA stacking of two silicene layers is preferred, in contrast to the AB stacking of graphite. This "on-site" positioning of the atoms in the top layer indicates the preference for two silicene layers with the same stoichiometry.

In the ML case the strain minimization has been found as an important construction principle for the geometries [27], which should also be important for the bilayer adsorbates. The experimental lattice constant of the $\sqrt{3} \times \sqrt{3}$ translational symmetry is equal to the measured STM spot distance, which is about 6.3 Å [28]. This value is close to the period 0.65 ± 0.01 nm derived from LEED spot distributions at low temperatures [18]. Together with the bulk Ag lattice constant $a_0 = 4.077$ Å [29], which is close to the theoretical vdW value $a_0 = 4.12$ Å, the strain for the corresponding bilayer systems grown on the 3×3 on 4×4 structure amounts to -5.6%. This is one of the reasons why the 3×3 on 4×4 system is unlikely to serve as a substrate for a bilayer with $\sqrt{3} \times \sqrt{3}$ symmetry in the topmost layer. We propose a bilayer translational symmetry combination, following the strain-minimization argument. This is the $(2\sqrt{3} \times 2\sqrt{3})R30^\circ$ bilayer silicene on $(\sqrt{19} \times \sqrt{19})R23.4^\circ$ silver substrate that gives a biaxial strain of only -0.2%.

Another argument for this proposal is the relative rotation of the $(2\sqrt{3} \times 2\sqrt{3})R30^\circ$ bilayer silicene on $(\sqrt{19} \times \sqrt{19})R23.4^\circ$ Ag(111) to surrounding silicene monolayer systems of the four observed symmetries $\sqrt{7} \times \sqrt{7}$ on $\sqrt{13} \times \sqrt{13}$, 3×3 on 4×4, 2×2 on $\sqrt{7} \times \sqrt{7}$, and $\sqrt{7} \times \sqrt{7}$ on $2\sqrt{3} \times 2\sqrt{3}$ by 9.5°, 23.4°, 4.3°, and 6.6°, respectively. From the experimental STM images of bilayer islands on monolayer silicene wetting layers [10,19,28], we derive the corresponding rough values of 10°, 24°, 5°, and 5°. The match of relative rotations is a further strong argument for the proposed bilayer geometry.

There is an additional argument suggesting a $(2\sqrt{3} \times 2\sqrt{3})R30^\circ$ bilayer phase on $(\sqrt{19} \times \sqrt{19})R23.4^\circ$ Ag(111). This adsorbate structure is close to the $(3.5 \times 3.5)R26^\circ$ spot arrangement seen in LEED patterns of bilayer silicene [28]. Indeed, experimentalists also conclude "that the $(2\sqrt{3} \times 2\sqrt{3})R30^\circ$ phase must correspond to the $(3.5 \times 3.5)R26^\circ$ phase" [28]. Recently, Jamgotchian *et al.* [6] investigated the structure of silicene on Ag(111) by means of LEED and STM measurements. They also claimed that the LEED pattern and STM images correspond to a $(2\sqrt{3} \times 2\sqrt{3})R30^\circ$ phase.

Results of the structural optimizations for monolayer and bilayer adsorbates with $(2\sqrt{3} \times 2\sqrt{3})R30^\circ$ on $(\sqrt{19} \times \sqrt{19})R23.4^\circ$ symmetries are shown in Figs. 1(a) and 1(b) as top and side views. The strong deformation of the fictitious $2\sqrt{3} \times 2\sqrt{3}$ monolayer system in Fig. 1(a) is remarkable, when comparing the monolayer system to the five monolayer systems [27] found to be metastable depending on the Si chemical potential. There is a clear tendency of the rearrangement of a ML silicene toward a triple layer of Si atoms. The bottom atomic layer of each silicene is remarkably buckled with amplitudes of 0.43 Å (lower silicene) or 0.72 Å (upper silicene) and can therefore split into two atomic layers. In addition, four of the 24 Si atoms in a unit cell in the uppermost

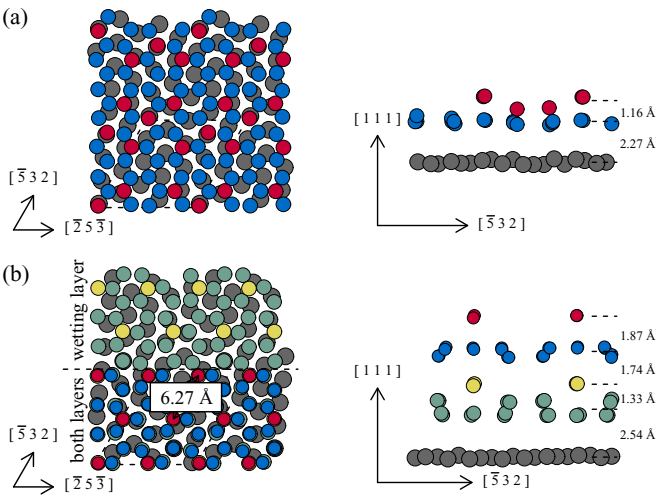

FIG. 1. (Color online) Top (left panels) and side (right panels) views of (a) monolayer and (b) bilayer silicene geometry $(2\sqrt{3} \times 2\sqrt{3})R30^\circ$ on $(\sqrt{19} \times \sqrt{19})R23.4^\circ$ Ag(111). Red (yellow) circles display outward buckled atoms, while blue (green) ones correspond to the bottom of a silicene layer. Silver atoms are represented as gray dots. For a better understanding, the top view of (b) also shows the wetting silicene layer besides the bilayer.

atomic layer of each silicene sheet have a larger distance to the bottom layer in comparison to typical buckling amplitudes of freestanding monolayer silicene. However, these atoms are not arranged in a $\sqrt{3} \times \sqrt{3}$ lattice in the monolayer case in Fig. 1(a).

The bilayer system in Fig. 1(b) clearly shows a similar lateral arrangement of the atoms in each of the two silicenes. The $(2\sqrt{3} \times 2\sqrt{3})R30^\circ$ bilayer silicene on the Ag(111)$(\sqrt{19} \times \sqrt{19})R23.4^\circ$ substrate system indeed exhibits an AA stacking in agreement with the general tendency for "on-site" positioning. The stacking result has been confirmed by additional computations, for instance by displacing the two silicene layers against each other to an AB stacking as starting geometry for the atomic relaxation. However, the system changes over into the AA configuration without energy barriers. The silicene atoms leave the high-symmetry positions of the underlying silver, which is a strong indication for a small Si-Ag interaction compared to the interaction between the two silicene monolayers. The hexagonal arrangement of the atoms in the silicene closer to the substrate is conserved. The top Si atoms of the uppermost silicene layer form a $\sqrt{3} \times \sqrt{3}$ lattice. Similar to the monolayer silicene, there is a tendency for splitting each layer into three sublayers of Si atoms. The buckling amplitudes of the two bottom sublayers are of the order of magnitude known for freestanding silicene. The corresponding vertical distances vary in the range of 1.3 to 1.9 Å, i.e., of values $d/\sqrt{3}$ or $d/\sqrt{2}$ with d as the bulk bond length between two covalently bonded silicon atoms. The distance of the lowest bottom layer to the Ag substrate amounts to 2.5 Å. This value is of the order of the sum of the covalent radii of Si (1.11 Å) and Ag (1.34 Å) [30] and, hence, indicates some covalent bonding between adsorbate and substrate. The generally more symmetric arrangement of Si atoms in each silicene layer in the bilayer system compared to the monolayer situation is obvious. Despite the slightly different arrangements of the Si atoms in the two silicene layers, their translational symmetries are the same with a resulting lattice constant of 12.66 Å [see Fig. 1(b)], which is equal to the measured distance of second nearest neighbor STM spots [10,28].

Each of the two silicene layers exhibits an interesting substructure. Together with three neighbors underneath each outstanding Si atom forms a small Si island of tetrahedron shape, that gives rise to a local trigonal symmetry. Practically, in one $2\sqrt{3} \times 2\sqrt{3}$ unit cell and each silicene four Si tetrahedra appear. As a consequence, the silicene bilayer system, peeled off the substrate, exhibits a $\sqrt{3} \times \sqrt{3}$ translational symmetry, because the $2\sqrt{3} \times 2\sqrt{3}$ unit cell decays into four smaller unit cells. This result of the structural optimization not only confirms the STM findings [10,28], including the corresponding measured lattice constant and symmetry, but also the LEED studies [28], assuming that the influence of the Ag substrate can be neglected. Indeed, the silver substrate plays only a minor role because of the small mean-free path of about 5 Å of the electrons with a kinetic energy of about 60 eV [25] used in the diffraction experiment.

As a freestanding system the peeled-off bilayer adsorbate is significantly modified during atomic relaxation. Despite the constrain of the $2\sqrt{3} \times 2\sqrt{3}$ translational symmetry substantial atomic displacements occur to make the BL system symmetric. This tendency especially holds for the atoms of the atoms of the wetting layer, which exhibit similar bucklings along the BL normal as in the former top silicene but with opposite sign.

B. Electronic structure

In the bilayer silicene adsorbate in Fig. 1(b), the arrangement of the uppermost outward displaced Si atoms gives rise to corresponding protrusions and, hence, spot arrangements in the STM images in Fig. 2. Indeed, a perfect $\sqrt{3} \times \sqrt{3}$ pattern is found in agreement with the experimental observations [10,19,28] for the minimum-energy silicene bilayer system. Independent of the sign of the bias voltage each spot covers one top Si tetrahedron. This is clearly shown by the distribution of the Si cores in Fig. 2. The main contributions to the spots can be traced back to tunneling out from the bonding states or into the antibonding states of the tetrahedron. As a consequence the empty-state and filled-state images are very similar. Also the spot distance of 6.33 Å is in excellent agreement with the measured value of 6.3 Å [28]. There are two other facts supporting this conclusion. The experimental STM scans [28] exhibit a large corrugation in the top bilayer silicene of 3 Å, while this value is reduced to about 2 Å in the monolayer system. Both values only slightly overestimate the structural parameters given in Fig. 1. The measured STM images [28] indicate a step height from the monolayer to the bilayer system of about 3 Å in rough agreement with the value of 3.6 Å in Fig. 1.

In order to understand the electronic properties of the silicene BL adsorbate system we investigate the band structure in Fig. 3(b). The BZs in Fig. 3(a) indicate that the positions K and K' of Dirac cones in the BZ of the freestanding silicene monolayer are folded onto the Γ point of the $(2\sqrt{3} \times 2\sqrt{3})R30^\circ$ BZ. The appearance of Si p_z-derived states above the Fermi level is obvious, although their highest contribution is mainly visible for bands in the energy range from $-0.6 \ldots -0.8$ eV near Γ or closer to the M and K points of the $2\sqrt{3} \times 2\sqrt{3}$ BZ. At about -0.22 eV the apex

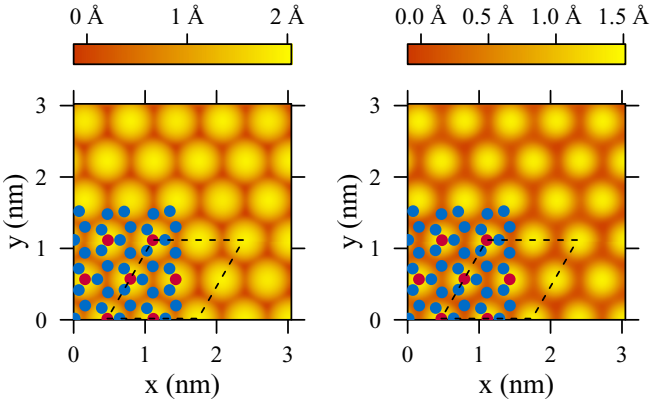

FIG. 2. (Color online) Filled-state (left) and empty-state (right) STM images of the $(2\sqrt{3} \times 2\sqrt{3})R30^\circ$ silicene bilayer on $(\sqrt{19} \times \sqrt{19})R23.4^\circ$ Ag(111) substrate. A bias voltage of ± 1 V is applied. The top view on the atomic cores is also displayed as red dots (most outward displaced atoms) or blue dots (Si atoms in the to lower atomic layers of the upper silicene).

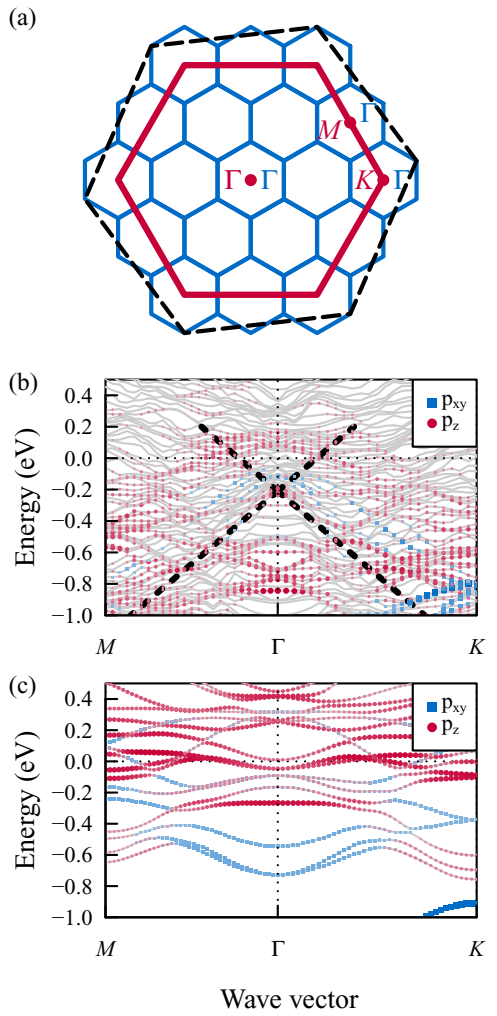

FIG. 3. (Color online) (a) BZ folding of the original 1×1 silicene geometry (red) onto the $(2\sqrt{3} \times 2\sqrt{3})R30^\circ$ structure (blue). The BZ of 1×1 silver is illustrated by dashed black lines. Band structures of (b) silicene BL on Ag(111) and (c) peeled-off silicene BL. In the case (b) conical linear bands corresponding to a Fermi velocity of 0.3×10^6 m/s and an apex position of -0.22 eV, as derived by ARPES, are indicated by black dashed lines to guide the eye. The strength of the Si p_{xy} and Si p_z orbital character of the bands is indicated by symbols of varying size and the saturation of color. The Fermi energy is chosen as energy zero.

of cone-shaped bands seems to occur. They are formed by Ag states which are hybridized with states of Si atoms closest to the substrate. The color of these bands in the energy interval $-0.2 \ldots -0.8$ eV in Fig. 3(b), i.e., the projection onto atoms, underline the Ag origin. The high density of the Bloch bands simulates a high intensity of emitted photoelectrons and may occur in ARPES measurements seemingly as linear bands. The corresponding linear bands, which have been made more visible by dashed lines, agree well with the ARPES data concerning apex position and Fermi velocity of 0.3×10^6 m/s [9,10]. However, apart from the apex itself the electronic states forming the conical linear bands are obviously Ag derived. We state a similar discrepancy between theory and the interpretation of experimental findings as in the monolayer case with 3×3 silicene on 4×4 silver(111) [11–17]. However, there is still agreement with the "measured" Fermi velocities, in particular that the Fermi velocity of the monolayer system is much larger compared to the BL results. In order to understand better the chemical nature of the conical linear bands the band structure of the peeled-off silicene bilayer is displayed in Fig. 3(c). No Dirac cones and Si p_z states appear around the Γ point below the Fermi level. There is a flat p_z-derived band at about -0.3 eV which is, however, clearly not cone shaped. A Dirac point only appears at 0.25 eV above the Fermi level. However, the crossing bands possess too small Fermi velocities to explain the experimental facts.

IV. SUMMARY

To conclude, by means of total-energy calculations in the framework of the density functional theory we have proposed a structural model for bilayer silicene on Ag(111). In contrast to the monolayer case, for a bilayer, the $(2\sqrt{3} \times 2\sqrt{3})R30^\circ$ translational symmetry is stable on the $(\sqrt{19} \times \sqrt{19})R23.4^\circ$ substrate. Such translational symmetries are not observed in the monolayer case. The bilayer system shows an AA stacking, and each silicene layer decays into a lower buckled system and significantly outward moved Si atoms. The translational symmetry of the isolated bilayer is however $(\sqrt{3} \times \sqrt{3})R30^\circ$ with smaller unit cells. The optimized atomic geometry of the adsorbate system yields properties in full agreement with experimental data: STM images, LEED spots, and ARPES measurements. However, the measured conical linear bands with apex position -0.22 eV below the Fermi level and a Fermi velocity of 0.3×10^6 m/s are explained by hybridized Ag states and not as Dirac cones derived from Si π states, very similarly to the monolayer case. This discrepancy requires further careful studies of the electronic properties of the bilayer adsorbate system. Furthermore, we suggest studies of the atomic geometry by means of dynamical LEED and the x-ray standing wave method.

ACKNOWLEDGMENT

This work has been initiated by discussions with Guy Le Lay and Patrick Voigt.

[1] S. Cahangirov, M. Topsakal, E. Aktürk, H. Şahin, and S. Ciraci, Phys. Rev. Lett. **102**, 236804 (2009).
[2] F. Bechstedt, L. Matthes, P. Gori, and O. Pulci, Appl. Phys. Lett. **100**, 261906 (2012).
[3] P. Vogt, P. De Padova, C. Quaresima, J. Avila, E. Frantzeskakis, M. C. Asensio, A. Resta, B. Ealet, and G. Le Lay, Phys. Rev. Lett. **108**, 155501 (2012).
[4] C.-L. Lin, R. Arafune, K. Kawahara, N. Tsukahara, E. Minamitani, Y. Kim, N. Takagi, and M. Kawai, Appl. Phys. Express **5**, 045802 (2012).
[5] L. Chen, C.-C. Liu, B. Feng, X. He, P. Cheng, Z. Ding, S. Meng, Y. Yao, and K. Wu, Phys. Rev. Lett. **109**, 056804 (2012).

[6] H. Jamgotchian, Y. Colignon, N. Hamzaoui, B. Ealet, J. Y. Hoarau, B. Aufray, and J. P. Bibérian, J. Phys.: Condens. Matter **24**, 172001 (2012).
[7] D. Chiappe, C. Grazianetti, G. Tallarida, M. Fanciulli, and A. Molle, Adv. Mater. **24**, 5088 (2012).
[8] B. Feng, Z. Ding, S. Meng, Y. Yao, X. He, P. Cheng, L. Chen, and K. Wu, Nano Lett. **12**, 3507 (2012).
[9] P. De Padova, P. Vogt, A. Resta, J. Avila, I. Razado-Colambo, C. Quaresima, C. Ottaviani, B. Olivieri, T. Bruhn, T. Hirahara, T. Shirai, S. Hasegawa, M. C. Asensio, and G. Le Lay, Appl. Phys. Lett. **102**, 163106 (2013).
[10] P. De Padova, J. Avila, A. Resta, I. Razado-Colambo, C. Quaresima, C. Ottaviani, B. Olivieri, T. Bruhn, P. Vogt, M. C. Asensio, and G. Le Lay, J. Phys.: Condens. Matter **25**, 382202 (2013).
[11] C.-L. Lin, R. Arafune, K. Kawahara, M. Kanno, N. Tsukahara, E. Minamitani, Y. Kim, M. Kawai, and N. Takagi, Phys. Rev. Lett. **110**, 076801 (2013).
[12] P. Gori, O. Pulci, F. Ronci, S. Colonna, and F. Bechstedt, J. Appl. Phys. **114**, 113710 (2013).
[13] Y.-P. Wang and H.-P. Cheng, Phys. Rev. B **87**, 245430 (2013).
[14] R. Arafune, C.-L. Lin, R. Nagao, M. Kawai, and N. Takagi, Phys. Rev. Lett. **110**, 229701 (2013).
[15] L. Chen, C.-C. Liu, B. Feng, X. He, P. Cheng, Z. Ding, S. Meng, Y. Yao, and K. Wu, Phys. Rev. Lett. **110**, 229702 (2013).
[16] S. Cahangirov, M. Audiffred, P. Tang, A. Iacomino, W. Duan, G. Merino, and A. Rubio, Phys. Rev. B **88**, 035432 (2013).
[17] Z.-X. Guo, S. Furuya, J.-i. Iwata, and A. Oshiyama, Phys. Rev. B **87**, 235435 (2013).
[18] L. Chen, H. Li, B. Feng, Z. Ding, J. Qiu, P. Cheng, K. Wu, and S. Meng, Phys. Rev. Lett. **110**, 085504 (2013).
[19] A. Resta, T. Leoni, C. Barth, A. Ranguis, C. Becker, T. Bruhn, P. Vogt, and G. Le Lay, Sci. Rep. **3**, 2399 (2013).
[20] G. Kresse and J. Furthmüller, Phys. Rev. B **54**, 11169 (1996).
[21] M. Dion, H. Rydberg, E. Schröder, D. C. Langreth, and B. I. Lundqvist, Phys. Rev. Lett. **92**, 246401 (2004).
[22] J. Klimeš, D. R. Bowler, and A. Michaelides, Phys. Rev. B **83**, 195131 (2011).
[23] L. Matthes, O. Pulci, and F. Bechstedt, J. Phys.: Condens. Matter **25**, 395305 (2013).
[24] G. Kresse and D. Joubert, Phys. Rev. B **59**, 1758 (1999).
[25] F. Bechstedt, *Principles of Surface Physics* (Springer-Verlag, Berlin, 2003).
[26] J. Tersoff and D. R. Hamann, Phys. Rev. B **31**, 805 (1985).
[27] P. Pflugradt, L. Matthes, and F. Bechstedt, Phys. Rev. B **89**, 035403 (2014).
[28] R. Arafune, C.-L. Lin, K. Kawahara, N. Tsukahara, E. Minamitani, Y. Kim, N. Takagi, and M. Kawai, Surf. Sci. **608**, 297 (2013).
[29] C. Kittel, *Introduction to Solid State Physics*, 8th ed. (John Wiley and Sons Inc., New York, Chichester, 2005).
[30] *Table of Periodic Properties of the Elements* (Sargent-Welch, Skokie, IL, 1980).